# Fluid-Structure Interaction Based Optimisation in Tidal Turbines: A Perspective Review

**Kulkarni, S., Wang, L., Golsby, N. & Lander, M**



DOI 10.1016/j.joes.2021.09.017
ISSN 2468-0133

Publisher: Elsevier

Journal of Ocean Engineering and Science 7 (2022) 449–461

Contents lists available at ScienceDirect

Journal of Ocean Engineering and Science

journal homepage: www.elsevier.com/locate/joes

# Fluid-structure interaction based optimisation in tidal turbines: A perspective review

Siddharth Suhas Kulkarni*, Lin Wang, Nicholas Golsby, Martin Lander

*School of Mechanical, Aerospace and Automotive Engineering, Coventry University, Coventry CV1 2JH, United Kingdom*

ARTICLE INFO

*Article history:*
Received 22 June 2021
Revised 24 September 2021
Accepted 24 September 2021
Available online 27 September 2021

ABSTRACT

Occurrences such as the global climate change have presented critical challenges to humanity and necessitated studies into how greenhouse gas emissions can be minimized. One practical solution is the generation of power from renewable and sustainable sources; hence, tidal current energy which, however, also gives rise to the concept of fluid-structure interaction (FSI). The pressure and fluid flow aspects affect the structural deformations and the structural deformations in turn affect pressure and flow. This paper presents a perspective review of FSI based optimisation in tidal turbines with a focus on low-order aerodynamic, computational fluid dynamics (CFD) and structural modeling. It was acknowledged that, to aid humanity amidst the issue of using renewable or non-renewable sources of energy, practical solutions such as generating renewable energy from sustainable sources are effective. Tidal current energy was found to be one of the most reliable solutions but further studies regarding its practicality was advised.



## 1. Introduction

Energy generation across the globe is still overly reliant on fossil fuels. Due to the burning of fossil fuels at an alarming rate, there is an increasing concern over the global climate change. Many policy makers worldwide have realised the importance of the energy generation through renewable sources. There are many renewable energy sources available such as hydropower energy, wind energy, geothermal and tidal energy [1]. In the past decades, the tidal turbine energy developed has attracted a lot of attention due to predictable nature of the tides, and has a great potential to generate clean energy [2]. The advances in the tidal energy, contribute fundamentally towards the sustainable power source focuses for 2050 and past, improvement of commercial wave and tidal arrays for producing more than 30 MW of power per annum would be required [3,4]. There are two primary forms of energy generation devices from tidal energy to electrical energy, namely tidal barrages (using potential energy) and tidal turbines (using kinetic energy) [5]. Although tidal energy has tremendous potential to generate electricity due to its predictable and renewable nature, the actual manufacturing of the tidal current turbines which should be efficient, and cost effective there is need for design optimisation to assess the turbine performance in terms of its design, layout and feasibility [6].

When designing tidal turbines, it is important to consider the fluid-structure interaction (FSI). FSI is defined as the Multiphysics coupling between laws describing fluid dynamics and structural mechanics, and it occurs when the flow of fluids causes the structure to deform [7]. Unlike most other forms of renewable energy, tidal currents are a reliable source of kinetic energy caused by the regular tidal cycles influenced by the moon's phases [8]. However, vibration in the tidal current turbines, which is induced by hydrodynamic forces, causes resonance and dynamic loads on the structure and results in structural deformation/failure. In turn, the deformation alters the boundary conditions of the fluid flow and, as noted by Trivedi & Cervantes [9], the phenomenon is characterised by either oscillatory or stable interactions between a moving or deformable structure and an internal or surrounding fluid flow.

Depending on the strains and stresses exerted on the solid objects (which is a function of the velocity and pressure of the flow as well as the material properties of the structure) the resultant deformations can be very small or significantly large [10]. If the structural deformations are very small and time variations are also relatively slow, then the deformation will not considerably affect the behavior of the fluid and, hence, the concern is only the consequential stress in the solid parts. In contrast, according to Nash

* Corresponding author.
*E-mail address:* ac8061@coventry.ac.uk (S.S. Kulkarni).

https://doi.org/10.1016/j.joes.2021.09.017

**Nomenclature**

| | |
|---|---|
| P | power (W) |
| T | thrust (N) |
| $\rho$ | air density (kg/m3) |
| A | rotor disc area (m2) |
| $F_L$ | lift force (N) |
| $F_D$ | drag force (N) |
| $F_A$ | axial force (N) |
| c | chord length (m) |
| $\lambda$ | tip speed ratio |
| $\Omega$ | angular velocity (m/s) |
| $\alpha$ | angle of attack (°) |
| $\varphi$ | inclination angle (°) |
| $\mu$ | shear viscosity (m2/s) |

& Phoenix [11], faster time variations can cause even otherwise negligible structural deformations to lead to pressure waves in the fluid which, in turn, cause the radiation of sound from vibrating structures. However, rather than and FSI problem, such a problem would be treated as an acoustic-structure interaction. Yet, if the structural deformations are large, the pressure and velocity aspects of the fluid will change, and the problem is then treated as a bi-directionally coupled Multiphysics analysis. According to Y. Li et al. [12] the pressure and fluid flow aspects affect the structural deformations and the structural deformations affect the pressure and flow. Kumar et al. [13] presented an optimisation method using the response surface model based on the surrogate models for radial basis function on the relative blade thickness to optimise the overall efficiency of the blade. Where Kumar et al. had used the SQP algorithm optimisation technique, Fatehi et al. [14] demonstrated the cavitation analysis based optimisation on the aerodynamic performance of the airfoils, to highlight that the stall and aerodynamic performance were notably improved when compared to without cavitation. A Blade Element Momentum Theory (BEMT) Model based design and optimisation performance of a vertical-axis tidal turbine blade was investigated by Mannion et al. [6] to employ the corrective methods for dynamic stall, flow expansion and finite aspect ratios.

The main objective of this paper is to conduct a comprehensive review on the FSI based optimisation in tidal turbines with a focus on low-order aerodynamic, computational fluid dynamics (CFD) and structural modeling. The previous research has highlighted different individual or combined optimisation techniques for the tidal turbine blade design and analysis.

However, single parameter optimisation increases the cost as well as computing resources, and only one parameter is varied at a single time or investigation of the fatigue life along with the tidal turbine blade performance as demonstrated by Ullah et al. [15]. Gao et al. [16] presented a comparative numerical analysis of combined wave and wind energy concepts but there was no FSI based optimisation conducted. FSI based optimisation plays an important role to save computational time, cost, and additional resources to obtain the optimal tidal turbine blade design. The multi-physics coupling of structural mechanics and fluid dynamics is described by FSI, hence it proves to be a very important tool to characterise the interaction between deformations of the tidal turbines and the fluid flow around it. Currently, there is a lack of a review on FSI based optimisation in tidal turbines. This paper has attempted to present a state-of-the-art review on the FSI based optimisation in tidal turbines, with a focus on low-order aerodynamic, computational fluid dynamics (CFD) and structural modeling. The future development is this area is also highlighted.

This paper is structured as follows. In Section 2, low order aerodynamic models, such as Actuator Disk Model and BEM model, are discussed. Section 3 presents different turbulence models involved in the CFD modeling along with their governing equations and different CFD discretisation methods. In Section 4, structural modeling techniques applied onto tidal turbine blade designs using 1D, 2D and 3D FEM models are described. FSI modeling techniques are discussed in Section 5, and the optimisation of tidal turbines through FSI are highlighted in Section 6. Section 7 presents the future areas of development, followed by conclusions in Section 8.

## 2. Low-order aerodynamic model

Low-order models are normally designed through modal truncation by using aeroelastic mode shapes of fully flexible wind turbines. To capture the effect of shed vorticity and dynamic stall, a fairly large number of aerodynamically dominated modes are needed because of the presumption of independent annular flow tubes in the Blade Element Momentum (BEM) theory [17]. Some of the low-order aerodynamic models include: actuator disk model, the BEM model, and the vortex model, which are discussed below.

### 2.1. Actuator disk model

The actuator disk model is a mathematical model used in developing ideal actuator disks that are mostly found on helicopter motors and propellers of aeroplanes [17]. The rotor of the actuator disk is usually modeled as an infinitely thin disc that has a constant velocity along the axis of rotation, i.e. the basic state of a hovering helicopter [18]. The disc is used in creating a flow around the rotor, which creates a mathematical relationship between the power, rotor radius, induced velocity and torque [19]. A number of studies have also considered the friction as one of the variables, arguing that it can affect torque under certain conditions, e.g. when a helicopter is moving [20,21].

Nonetheless, for a stationary rotor, e.g., a hovering plane, the power needed to produce a certain thrust using the actuator disk model is calculated as:

$$\boldsymbol{P} = \sqrt{\frac{\boldsymbol{T}^3}{2\boldsymbol{\rho A}}} \tag{1}$$

where $P$ is the power, $T$ is the thrust, $\rho$ is the air density, and $A$ is the rotor disc area.

An illustration of the actuator disk model is depicted in Fig. 1.

The real-life application of devices that convert translation energy into rotational energy include marine and aviation propellers, helicopter rotors, windmills, wind turbines, centrifugal pumps, turbochargers, etc. [23,24].

### 2.2. BEM (blade element momentum) model

The BEM model is a combination of the blade element theory and actuator disk model in order to calculate the local forces on a wind turbine blade or a propeller. An illustration of the BEM model is depicted in Fig. 2. It divides the blade into a series of elements then calculates the forces on each element. Adding together the forces of the different elements enables the calculation of the entire momentum produced by the entire rotor or propeller [25]. The separation of the elements alleviated the historic challenge of calculating the induced velocities at the propeller or rotor [26].

The BEM model offered additional relationships that helps explain the induced velocity on the rotor disk. The induced velocity of the rotor is calculated as:

$$\upsilon_i = \sqrt{\frac{T}{A}\cdot\frac{1}{2\rho}} \tag{2}$$

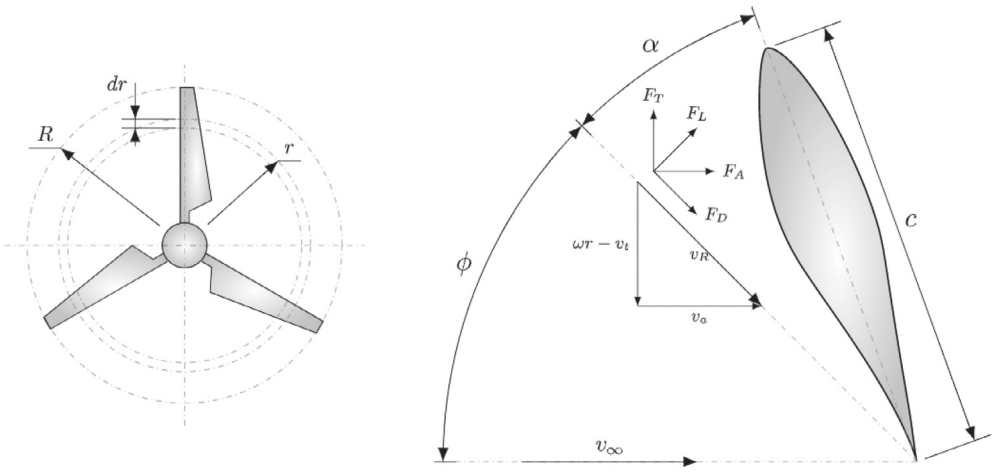


where, $F_L$, $F_D$, $F_A$ and $F_T$ are the lift, drag, axial and tangential forces respectively, $c$ is the chord length, $v_a$, $v_t$ and $v_R$ are the axial, tangential and resultant velocity respectively, $\omega$ is the angular velocity, $\alpha$ is the angle of attack and $\varphi$ is the flow inclination angle.

**Fig. 1.** Generated actuator discretisation scheme [22].

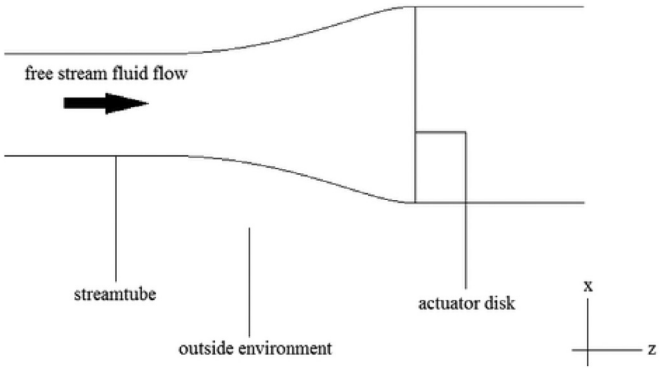


**Fig. 2.** BEM Model [27].

where $\upsilon_i$ is the induced velocity, $P$ is the power, $T$ is the thrust; $\rho$ is the air density, and $A$ is the rotor disc area.

If this method is used in rotors in forward motion, Madsen et al. [26] recommend that one should consider the flapping motion of the blades in addition to the lateral and longitudinal distribution of the induced velocity of the rotor using harmonic models.

### 2.3. Vortex model

Before explaining how the vortex model helps in understanding FSI-based optimisation in tidal turbines, it is important to first discuss what a vortex is. A vortex refers to a region within a fluid wherein the flow revolves around an axis line that is curved or straight. Vortices can be seen as whirlpools, smoke rings, dust devils, tornados and/or tropical cyclones [28]. A key concept regarding the dynamics of vortices is the vorticity, a vector describing the local rotary motion at a point within the fluid, which moves along with it, as would be seen by an observer [29,30].

In theory, the speed $u$ of the particles, i.e. the vorticity in a vortex, which helps move a tidal turbine, might vary with the distance $r$ from the axis in a number of ways, including (1) the fluid rotating like a rigid body, and (2) the particle speed being inversely proportional to the distance from the axis [31]. The fluid tends to rotate like a rigid body when the angular rotational velocity $\Omega$ is uniform causing speed $u$ to increase proportionally to distance $r$ from the axis. This means the vorticity will be similar everywhere, i.e. the direction will be parallel to the rotation axis and the magnitude equals to twice the uniform angular velocity $\Omega$ of the fluid adjust to the rotational centre as depicted below [32–34]:

$$\vec{\Omega} = (0,\ 0,\ \Omega),\ \vec{r} = (x, y, 0) \tag{3}$$

$$\vec{v} = \vec{\Omega} \times \vec{r} = (-\Omega y, \Omega x, 0) \tag{4}$$

$$\vec{v} = \vec{\nabla} \times \vec{u} = (0, 0, 2\Omega) = 2\vec{\Omega} \tag{5}$$

When the speed $u$ of the particle is inversely proportional to distance $r$ from the axis, then there would be no rotation as objects would maintain a similar orientation while moving in circles around the axis of the vortex [35] as depicted below:

$$\vec{\Omega} = \left(0,\ 0,\ \alpha r^{-2}\right),\ \vec{r} = (x, y, 0) \tag{6}$$

$$\vec{v} = \vec{\Omega} \times \vec{r} = \left(-\alpha y r^{-2}, \alpha x r^{-2}, 0\right) \tag{7}$$

$$\vec{w} = \nabla \times \vec{u} = 0 \tag{8}$$

## 3. CFD (computational fluid dynamics) modeling

Using digital computers, the science of CFD produces quantitative predictions of the phenomena of fluid flow phenomena based on the conservation laws, which are concerned with the conservation of mass, momentum and energy that govern the fluid motion [36]. The elementary basis of the CFD problems is the Navier-Stokes equations that define single-phase fluid flows for liquid or gas but, most importantly, not both. According to Lindstrom et al. [35], these equations are simplified by removing terms that describe viscous actions to yield Euler equations while the full potential equations are arrived at by further simplification through the removal of terms that describe vorticity [37]. Vorticity has been described as the curl of the flow of velocity [38].

### 3.1. Governing equations

The fundamental governing equations of fluid dynamics (continuity, : and energy equations) are the cornerstone of CFD. According to Constantin et al. [37], these equations are mathematical statements of three fundamental properties on which all fluid

dynamics is founded, which are: (i) energy is conserved, (ii) mass is conserved, and iii) *F(force) = m(mass) X a(acceleration)*, which describes Newton's second law. A continuity equation is perceived as a nonlinear diffusion equation with regular drift term [39]. It inspires ubiquitous applications in fields such as curve measurement analysis, crowd modeling, biomedical imaging and prediction of aerospace debris cloud evolution [40,41] . A continuity equation is either treated as a Cauchy problem or initial boundary problem [42]. The elementary physics of continuity equations is the conservation of mass principle, which is defined as the conservation law the rate at which mass changes within a control volume is equivalent to the net rate of mass flowing into the control volume [43]. Navier-Stokes equations (momentum equations) originated from Newton's second law which states that a moving object's force is equivalent to its rate of change of momentum.

### 3.2. Turbulence model

Turbulence modeling refers to the construction and application of mathematical modeling to predict the implications of turbulence [44]. Turbulent flows are common in nearly each and every real-life scenario, including airflow over aircraft wings [45]. Despite the years of research, there is no single analytical theory explaining the evolution of turbulent flow, only equations, which can be solved directly for simple cases of flow [44,46]. Turbulence models can be roughly categorised into four groups, i.e., (1) RANS (Reynolds-Averaged Navier-Stokes), LES (Large Eddy Simulation), DES (Detached Eddy Simulation) and Hybrid models, which are illustrated below.

#### 3.2.1. RANS (Reynolds-Averaged Navier-Stokes)

The RANS equation, which stands from Reynolds-Averaged Navier-Stokes, is a time-averaged equation of fluid flow motion. It was first proposed by Osborne Reynolds, an innovator of fluid dynamics and one of the founders of the University of Manchester [47]. The equation is mainly used in describing turbulent flows and they can be applied with approximations rooted on knowledge of the properties of flow turbulence in order to approximate the time-averaged solutions of the Navier-Stokes equations [48]. The equation is written as follows for a stationary flow of an incompressible Newtonian fluid [49]:

$$\rho u_i \frac{\partial \overline{u_i}}{\partial x_i} = \rho \bar{f}_i + \frac{\partial}{\partial x_i}\left[-\bar{p}\delta_{ij} + \mu\left(\frac{\partial \overline{u_i}}{\partial x_j} + \frac{\partial \overline{u_j}}{\partial x_i}\right) - \rho\overline{u_i' u_j^i}\right] \quad (9)$$

where $-\rho\overline{u_i' u_j^i}$ is the apparent stress, $u_i$ is the fluctuating velocity component, $\bar{f}_i$ is the vector representing external forces, $\mu(\frac{\partial \overline{u_i}}{\partial x_j} + \frac{\partial \overline{u_j}}{\partial x_i})$ is the turbulent dissipation rate, $\rho$ is the fluid density, $\mu$ is the shear viscosity of the fluid.

The left side of the above equation denotes the change in mean momentum of the fluid element due to unsteadiness of the mean flow and the convection by the mean flow [50]. The change is, nonetheless, balanced by the following factors: the mean body force, the viscous stress, the isotropic stress and the apparent stress [51]. One of the major disadvantages of this model is that the nonlinear stress term requires additional modeling leading to more equations that are yet to be verified [52]. The Reynolds decomposition is the basic tool needed for the derivation of the RANS equation from the instantaneous Navier-Stokes equations [53].

#### 3.2.2. LES (Large Eddy Simulation)

LES is a mathematical model for the turbulence used in understanding fluid dynamics, which was first proposed by Joseph Smagorinsky in 1963 to simulate atmospheric air currents [54]. The simulation requires one to resolve a wide variety of length and time scales that affect the flow field using Navier-Stokes equations.

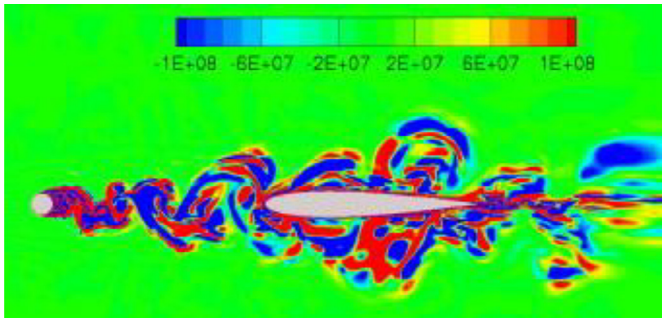


**Fig. 3.** DES Model [62].

Another approach is to use the direct numerical simulation (DNS), but it is overly expensive plus it prohibits simulation of practical engineering systems that have complex flow configurations or geometry, e.g., landing gears, vehicles, pumps, and turbulent jets among others [55,56]. LES was developed to decrease the computational cost by overlooking the smallest length scales that are expensive to resolve through low-pass filtering of the Navier-Stokes equations [57].

The LES model can be used on a temporal or spatial field $\emptyset\ (x,\ t)$ and execute either or both a temporal and a spatial filtering operation. The filtered field that is represented with a bar can be defined as follows [58]:

$$\overline{\emptyset\ (x,\ t)} = \int_{-\infty}^{\infty}\int_{-\infty}^{\infty} \emptyset\ (r, T)G(x-r,\ t-r)d\tau dr \quad (10)$$

where $G$ is the filter convolution kernel, $\emptyset\ (x,\ t)$ is the spatial and temporal field, $\tau$ is the stress tensor.

Eq. (10) can also be written as follows:

$$\overline{\emptyset} = G * \emptyset \quad (11)$$

The $G$ filter kernel has a $\Delta$ associated cut-off length scale and a $\tau_c$ cut-of time scale, and smaller scales are eliminated from the $\overline{\emptyset}$. It should also be noted that LES filtering operations cannot satisfy the LES operator [59].

#### 3.2.3. DES (Detached Eddy Simulation)

DES is a modified RANS model that uses a sub-grid scale formulation to execute LES calculations. Regions where the turbulent length scale less compared to the maximum grid dimension, i.e., regions near solid boundaries, are given the RANS mode of solution [60]. They are assigned the LES mode when the turbulent length exceeds the grid dimension, implying that the grid resolution is not as challenging as the pure LES, thus significantly reducing the cost of computation [61]. Fig. 3 presents a sketch of the DES model illustrating how RANS and LES are combined to form the DES model.

Lei et al. [61] reported that the DES model was first developed for the Spalart-Allmaras model, but later implemented to other RANS models by modifying the length scale that can either implicitly or explicitly be involved in the RANS model. This, however, does not overlook the fact that such studies as Song et al. [45] and Pakzad [52] consider the DES model more complicated than RANS or LES because of the RANS-LES switch during the simulation.

#### 3.2.4. Improved Delayed Detached Eddy Simulation (IDDES)

Although the LES and DES are often considered as high-fidelity turbulence models, they come with an enormously high computational cost to obtain good results [63]. Therefore, a combination of the RANS turbulence model and LES i.e., IDDES enables a high fidelity computationally more efficient method to analyze the computational performance of the turbine blades [64]. In determining

the pressure coefficient, Improved Delayed Detached Eddy Simulation captures the time-varying fluctuations pertaining to blade generated turbulence [65]. This model predicts more plentiful and realistic vortex structures which has impact on accurate determination of blade pressure distribution and also energy dissipation rate and downstream flow field [61]. Although this method hasn't been popular in the tidal turbine industry for numerical simulations, it is highly popular in the wind turbine industry due its nature to predict the accurate pressure fluctuations [66].

#### 3.2.5. Hybrid

Several studies have evaluated the ability of a hybrid RANS and LES turbulence method that can accurately predict the physics of an uneven separated flow field in an unstructured legacy [67]. In Wang et al. [66], the hybrid model blends the $k-\omega$ SST RANS model with a single equation LES model for the sub-grid scale turbulent kinetic energy $k^{sgs}$. The researchers found that the unstructured grids created by the hybrid model offer better resolution of the complex geometries that increase the efficiency of the hybrid. In Li and Huang [67], the RANS and LES hybrid was informed by an auxiliary transport variable $\tilde{B}$, executed in a compressible, high-order computational solver Flamenco. A flow around a NACA4412 aerofoil was used to evaluate the predictive capability of the hybrid model in adverse pressure gradients. The hybrid model responded well with increased resolution; predicted cylinder separation angles were in line with the expected range, despite the difficulties in accurately capturing the recirculation lengths.

### 3.3. Discretisation method

Generally, the stability of the chosen discretisation is numerically established rather that analytically. Discretisation entails taking continuous variables or functions and transforming them into, respectively, discrete variables or functions [68]. Since it is considerably manageable to analyze discrete data and functions those continuous ones, discretisation is usually the first step in many analyzes. The discretisation process can be visualised as: (i) analysing the continuous values taken on by a variable, (ii) dividing the continuous values into segments, and iii) grouping the segments into bins by first deciding how the number of bins should be selected and then deciding how wide they will be [69,70]. The discretisation methods can be roughly categorised into three groups, i.e., FVM (Finite Volume Method), FEM (Finite Element Method) and FDM (Finite Difference Method), which are illustrated below.

#### 3.3.1. FVM (Finite Volume Method)

FVM features an advantage in memory usage and solution speed, which makes it a commonly used approach in CFD codes especially for large problems, source term dominated flows and high Reynolds number turbulent flow [71]. The governing partial differential equations in this model (usually the Navier-Stokes equations, the turbulence equations and the mass and energy conservation equations) are conservatively recast and solved over discrete control volumes [72]. Such discretisation ensures the conservation of fluxes via a particular volume control.

#### 3.3.2. FEM (Finite Element Method)

Although FEM is normally used in the structural analysis of solids, it is also applied to fluids, but special care is required in its formulation to ensure a conservative solution. However, even with the need to formulate it carefully in order to ensure it is conservative, FEM is more stable than the FVM model even though it may require more memory and has relatively slower solution times [73].

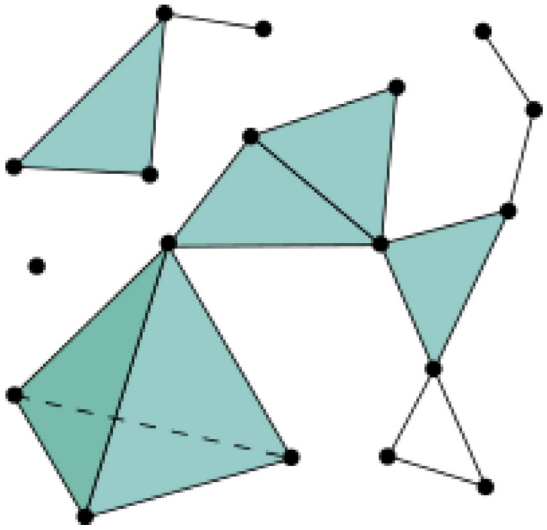

**Fig. 4.** Simplicial Complex [75].

#### 3.3.3. FDM (Finite Difference Method)

FDM is simple to programme but is presently used only in limited specialised codes that handle complex geometry with high efficiency and accuracy by using overlapping grids or embedded boundaries [74].

### 3.4. Mesh

Mesh refers to a subdivision of a continuous geometric space into a discrete topological and geometric cell forming a simplicial complex [75]. A simplicial complex is a set composed of triangles, line segments, points, and their n-dimensional counterparts, as illustrated in Fig. 4.

#### 3.4.1. Structured mesh

Nash & Phoenix [11] define a structured mesh as a set of hexahedral elements with an implicit connectivity of the points in the mesh. The generation of the structured mesh for complex geometries is time-intensive because of the possible need to manually break the domain into several blocks depending on the nature of the geometry. Because the structured mesh can handle cells with very high aspect ratio cells in the boundary layer, it has superior accuracy for viscous calculations. An example of structured mesh is depicted in Fig. 5.

#### 3.4.2. Unstructured mesh

An unstructured is a set of elements, usually tetrahedrons, with a connectivity that is explicitly defined. The process of generating an unstructured mesh involves, first, creating the points and, second, defining the connectivity between the points [77,78]. Because of its automation and flexibility, the unstructured mesh is a favoured choice even though it may have a relatively unfavourable solution accuracy compared to the structured mesh. This, according to Ji et al. [77], is because of the presence of skewed elements in sensitive areas such as boundary layers. An example of unstructured mesh is depicted in Fig. 6.

#### 3.4.3. Hybrid mesh

The hybrid mesh generation is an attempt to combine, exploit and enhance the advantages of the structured and unstructured meshes [80]. In the hybrid mesh, the viscous region is filled with hexahedral or prismatic cells while the remaining domain is filled with tetrahedral cells. Hybrid meshes in viscous regions have been

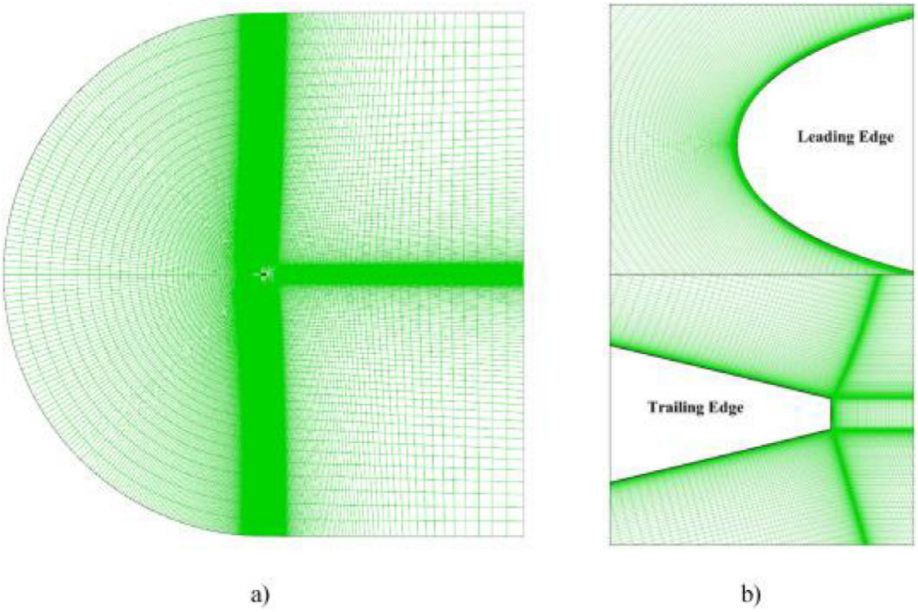


**Fig. 5.** Structured mesh on a 2D airfoil [76].

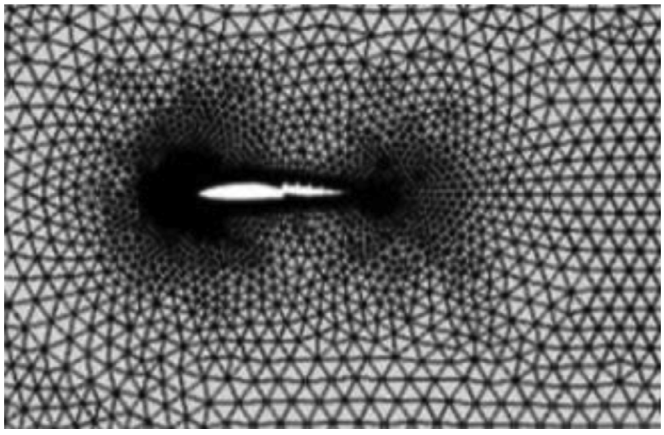

**Fig. 6.** Unstructured mesh around an airfoil [79].

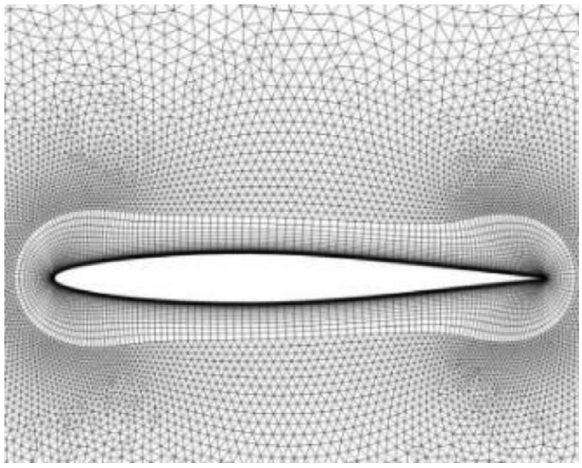

**Fig. 7.** Hybrid mesh [83].

observed to create lesser numbers of elements than fully unstructured meshes with similar resolutions, which is demonstrated in Fig. 7 [81]. Because the hybrid mesh does not have restrictions on the number of faces on a cell or edges, it is highly flexible and suitable for topological adaptation. It has also been reported that the unstructured mesh has an advantage over its structured counterpart in handling complex geometries, load balancing using graph partitioning algorithms, mesh adaptation using local refinement and de-refinement and moving mesh capability by locally repairing poor quality elements [82].

### 3.5. Boundary conditions

Boundary conditions in fluid dynamics refer to the set of constraints to boundary value problems in computational fluid dynamics, including inlet and outlet boundary conditions, periodic or cyclic boundary conditions, symmetric boundary conditions, axisymmetric boundary conditions, constant pressure conditions, and wall boundary conditions [84]. Boundary conditions for fluid flow are essentially more complex due to the coupling of velocity fields with pressure distribution [85]. Defining the perfect conditions in CFD requires the specification of two types of boundary conditions including the Neumann boundary condition and the Dirichlet boundary condition. The Dirichlet boundary condition $\emptyset$ is the requirement for specifying the physical quantity compared to the boundary of a turbulent flow, illustrated as follows:

$$\emptyset = f\ (analytic) \tag{12}$$

The Neumann boundary condition, on the other hand, involves the prescription of the derivative boundary, as illustrated below: $\frac{\partial \emptyset}{\partial n} = 0$. Inflow boundaries mainly assume the Dirichlet approach, whereas outflow boundaries mainly assume the Neumann approach [86]. Illustrations of inflows and outflows can be seen in Fig. 8 below:

## 4. Structural modeling

Structural modeling is a diverse set of mathematical models, computer algorithms and statistical techniques, which turn networks of constructions into data [88]. The structural strength of the tidal turbine blade system is driven by the material properties, hydrodynamic shape and the types of loads it can withstand [89,90]. The structural modeling approaches of the tidal turbine blades ensure that the system can meet the static as well as the dynamic load based fatigues from the marine currents over its lifetime [91].The three types of structural modeling approach that will

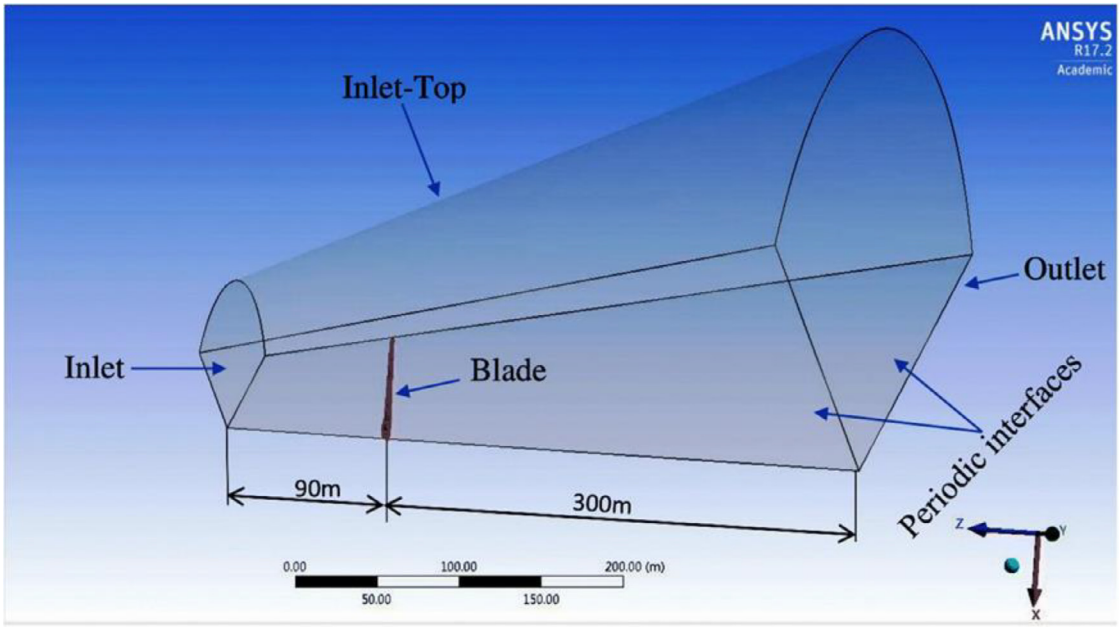


**Fig. 8.** Boundary Condition in a CFD simulation [87].

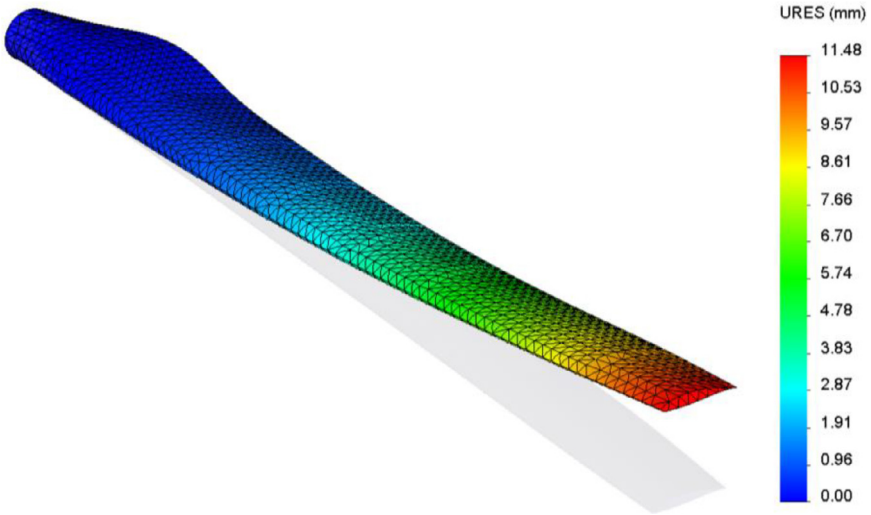


**Fig. 9.** Maximum deflection on a blade using FEM [94].

be discussed in this file is 3D FEM model and the 1D & 2D beam models.

### *4.1. 3D FEM Model*

3D FEM models were developed after researchers realised that even though there are numerous geotechnical problems, which can be reduced to plane strain or axisymmetric conditions, others are overly challenging, which can simply be understood by using different three dimensional methods [92,93]. Applying the plane strain or axisymmetric model by reducing a particular direction to zero is merely simplifying the real case and can be shown in Fig. 9 below.

Ye et al. [93] conducted a hydrodynamic analysis on the design of the nozzle turbine to analyze the pressure effects and evaluate the durability of the composite material on the turbine under critical hydrodynamic and hydrostatic pressure loads with a failure criterion implementation. Payne et al. [94] studied the fatigue load damages on a horizontal axis tidal turbine blade which are caused due to the wave loads in order to avoid the entire turbine replacement cost, by performing 3D FEA on the parameter variation such as pitch angles, blade material, and number of blades to ensure the structural stability of the turbine system. A finite vortex method employing the Kutta condition of the pressure difference at the trailing edge of a cycloidal vertical axis tidal turbine was developed by Nachtane et al. [95] to compare the instantaneous and average loads of the fixed pitch turbine and cycloidal turbine.

It is important to consider every component is geotechnical problems, particularly when the domain has an irregular shape because a corner effect can have a significant influence of how structures behave [96].

### *4.2. 1D and 2D beam model*

A 1D beam model is easier and computationally more effective compared to the 3D FEM model, which is why it is extensively used for different engineering applications to carry out static and dynamic analysis of structures [97]. 1D beams have seven at every

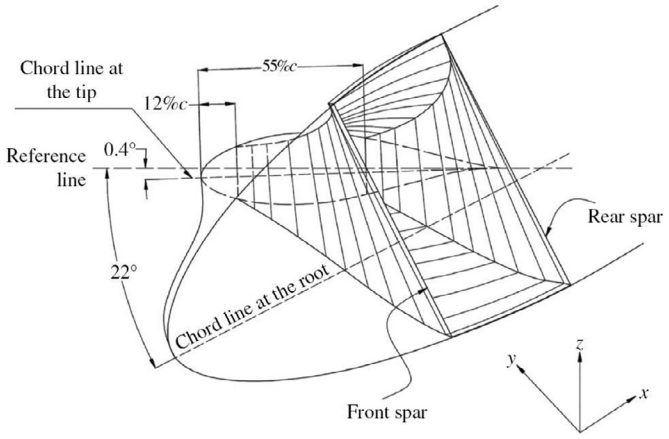


**Fig. 10.** Isometric view of a hydrodynamic twisted cantilever airfoil beam [101].

end of the node, i.e., one DOF approximating the cross-sectional deformation because of torsional warping, three rotations *(R)* and three translations *(T)* [98]. 2D beam models are useful to characterise the complexity of the rotating blade systems to adopt them into modal reduction of the beam elements [99]. 2D beam finite elements are assumed to be axis symmetrical, and also has the flexibility to represent the modal density not represented by 1D beam kinematics [100]. The kinematics of the rotating tidal turbine blade when describing them through a beam model are often assumed that the blade structure is made of an isotropic material and the model has a twisted cantilever beam fixed at the blade root level. Nguyen et al. (n.d.) presented an isometric view of the twisted cantilever beam of a twisted hydrofoil made out of two spars and two skins as where the thrust force was assumed to be acting at the centre of the hydrodynamic tidal turbine blade, and is highlighted in Fig. 10 below:

## 5. FSI modeling

FSI refers to the interaction of movable or deformable structures within or around a fluid flow, i.e., the interaction between fluids and solids [102]. Such interaction is a phenomenon that one can observe in nature, e.g. the movement of sand dunes and the deformation of trees caused by wind. Such a process can be calculated using equations and laws from different physical disciplines, e.g., Multiphysics applications such as FSIs [103]. FSI simulations are essentially classified into monolithic and partitioned methods and partitioned methods are further classified into one-way and two-way modeling [27,104].

### 5.1. One-way FSI and two-way FSI

In one-way modeling, the property of a particle flow in the fluid affect such properties of the particle as temperature, velocity, etc., but the particle hardly influences the properties of the fluid [105]. In two-way modeling, there is mutual interaction between the particles and the fluid, i.e., they body affect each other's properties. Irrespective of whether one-way or two-way modeling methods are applied, the solutions are derived from a partitioned approach wherein separate solutions from the numerous physical fields are prepared [106]. For one-way modeling, on the pressure of the fluid that acts at the structure is transferred to the structure solver whereas, in two-way modeling, the displacement of the structure is transferred to the fluid solver, as well [107].

Fig. 11 below is an illustration of the one-way modeling approach. The fluid field is normally solved when fulfils the convergence criteria then the transfer of the calculated forces at the

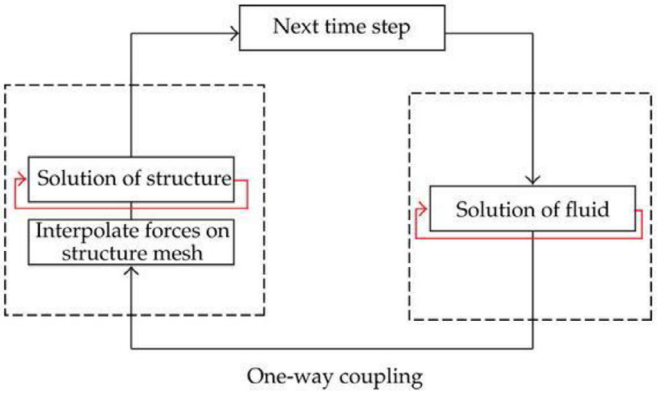


**Fig. 11.** One-Way FSI [103].

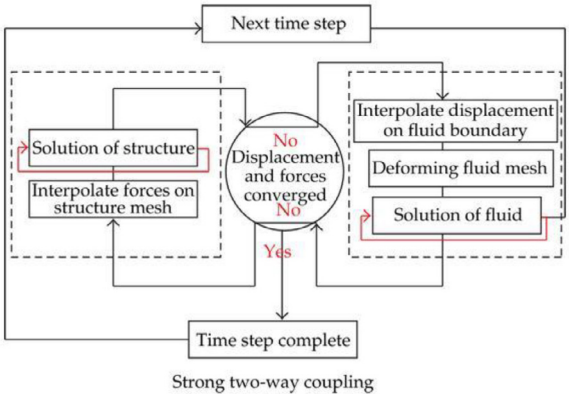


**Fig. 12.** Two-Way FSI [103].

structure boundaries to the structure side commences. The structure side is also calculated when convergence criteria is met, and the fluid flow calculated to convergence. The solution is fulfilled once one reaches the maximum number of time steps.

Fig. 12 below illustrates a process flow chart of the two-way modeling approach. As can be seen from Fig. 12, a converged solution for the flow field is needed to create the forces acting on the structure. A converged solution of the structural dynamics is also attained after interpolating the fluid mesh forces to the surface mesh of the structure. The structure's response to the load represents a structural grid nodes displacement.

### 5.2. Continuum and discrete modeling

Continuum elements essentially model small blocks of materials in a component. The discrete model, on the other, takes into consideration the individual existence of each discrete grain forming the medium. In discrete modeling, the collection of grains is essentially influenced by standard equations of motion as well as the contact laws that describe the collisions between surfaces [108].

#### 5.2.1. FSI formulation at continuum level

The FSI formulation at continuum level uses a fixed Euler coordinate system comprising of the following: a conservation of mass and momentum, phase convection equation and constitutive laws for stress as data [109]. The stress implied is the Cauchy stress, which is also known as laboratory stress, and the phase variable is applied in defining such material data as constitutive law for the material and stress parameters [110]. The mass, momentum and energy conservation equations are presented in Eqs. (13)–(15), re-

spectively:

$$D_t\rho + D_{xi}\left(u_j\rho\right) = 0 \tag{13}$$

$$D_t m_i + D_{xi}\left(u_j m_i\right) = D_x\sigma_i \tag{14}$$

$$D_t e + D_{xi}\left(u_j e\right) = D_x\sigma_i u_i \tag{15}$$

The phase convection equation is given by

$$D_t\theta + D_{xi}u_i e = 0. \tag{16}$$

*5.2.2. ALE-VMS formulation of fluid mechanics with weak boundary conditions*

The ALE-VMS formulation of fluid mechanics with weak boundary conditions is given by $u^h \in S_u^h$ and $p^h \in S_p^h$, such that $VW^h \in V_u^h$ and $Vq^h \in V_p^h$. The time-dependent fluid domain is first split into individual spatial finite element subdomains and the $S_u^h$ and $S_p^h$ that respectively denote the finite element spaces velocity and pressure, and the $V_u^h$ and $V_p^h$ test functions are of equal order comprised of piece-wise linear polynomials that are also continuous at the inter-element boundaries of the model [111].

*5.2.3. Sliding-interface formulation for objects in relative motion*

This model is derived from the fact that fluid meshes surrounding a solid structure can slide over each other to accommodate a rotational motion of the solid; also, a fluid mesh adjacent to the sliding interface can translate through a background fluid mesh. Owing to independent nature of the design of fluid and solid meshes as well as the relative motions of sliding fluid meshes, non-matching meshes can take place at their common interfaces. Such non-matching meshes are normally connected by variable-node elements thus guaranteeing continuity, compatibility and force equilibrium in all the interfaces [112].

*5.2.4. Time integration of FSI equations*

Primarily, time integration of FSI equations intends to control the following error

$$g_{n+1} = x(t_{n+1}) - x_{n+1} \tag{17}$$

such that,

$$||g_{n+1}||L_2 \leq \varepsilon_g^{\Delta t} \tag{18}$$

holds with a user-given tolerance $\varepsilon_g^{\Delta t}$ for the error and with the $L_2$-norm expressed as:

$$||(.)||L_2 = \sqrt{\int_\Omega (.)^2} \tag{19}$$

Because the error is ever accessible directly, controlling it is practically impossible. The only alternative is using the local error defined as:

$$I_{n+1} = x(t_{n+1}) - x_{n+1} \tag{20}$$

whereby one assumes $x_n = x(t_n)$ as the start of the time step [108] as illustrated in Fig. 13 below:

## 6. FSI-based optimisation of tidal turbines

Oceanic tides can produce vast amounts of renewable energy and tidal turbines are one of the vital technologies that can extract and harness such a potential. To harness economically effective amounts of power, thousands of tidal turbines need to be deployed in the ocean, but this has led to questions regarding the manner in which they should be displayed in order to harness maximum [113]. This section will discuss FSI-based optimisation of both tidal turbine airfoils and blades.

### 6.1. FSI-based optimisation of tidal turbine airfoils

The deformation of airfoil is due to its interaction with the forces imposed by the fluid surround the airfoil, the airfoil's material properties, stiffness distribution or mass, as well as the actuation of the airfoil. When an aircraft is moving, the forces passively interact to crease temporal and spatial patterns of airfoil shape and movement [114]. Fig. 14 below illustrates an aircraft's airfoil.

The FSI equation for optimising the tidal turbine airfoil is as follows:

$$\rho\left(\frac{\partial ufluid}{\partial t}\right) + \rho(ufluid\ .\nabla)ufluid = 0 \tag{21}$$

$$\nabla.\left[-PI + u\left(\nabla ufluid + (ufluid)^T\right) - \frac{2}{3\mu(\nabla * \text{ufluid})}\right] 1 + F \tag{22}$$

$$\frac{\partial\rho}{\partial t} + \nabla * (pufluid) = 0 \tag{23}$$

$$\rho\left(\frac{\partial^2 usolide}{dt^2}\right) - \nabla\ .\ \sigma = Fv \tag{24}$$

Kim et al. [113] studied the material fatigue effects produced due to the cyclic loads caused by the drag associated on the NACA0018 airfoil, and also investigated the parameters of the oscillation frequency and tip speed ratio. The results indicated that the high tip speed rations occur in the dynamic flow regimes where the blades not only create higher thrust but also peak-to peak cyclic normal force variations. The FSI analysis carried out by Zullah et al. [114] dealt with an oscillating airfoil to describe the vertical displacement and rotational displacement at the end of the each heave cycle. The results demonstrated that a higher angle of attack generates more hydrodynamic forces, but at the same time it requires more energy to carry out the pitch rotation, thus resulting in less turbine efficiency. A fully coupled 2D fluid-structure interaction simulations were investigated by Jeanmonod & Olivier [115] at Reynolds number of 1,100 with the airfoil chord ratio thickness of 1% (see Fig. 15) – for three different mesh configurations The results indicated that the pressure driven deformations increase the energy performance of the foils where the inertia-driven deformations are useful to the rear foils of the plate.

Further studies have demonstrated that in order to optimise the single turbine efficiency using the 2D airfoil shape parameterisation improves the overall efficiency by more than 20% when CFD is coupled with an optimiser such as Genetic Algorithms [117,118].

### 6.2. FSI-based optimisation of tidal turbine blades

Tidal turbine blades, on the other hand, go through considerable deflection because of fluid interactions and FSI models can help model such hydro-elastic behavior [119]. The blade is normally split into a number of independently functioning 2-dimensional parts whose aerodynamic forces can be summed based on the blade length to determine the total forces and moments on the rotating body [120]. The FSI-based optimisation allows one to calculate the forces on every part based on the local incident flow angles making use of knowledge on lift and drag characteristics of the blade numerically and empirically using the Reynolds number depending on the blade as well as the flow regime. Another method suggested by Zullah & Lee [112] is equating the decrease in pressure across the plane of the disk to the drag force or thrust on the rotor disk; thus, with a complementary assumption regarding the turbine efficiency, average rotational and

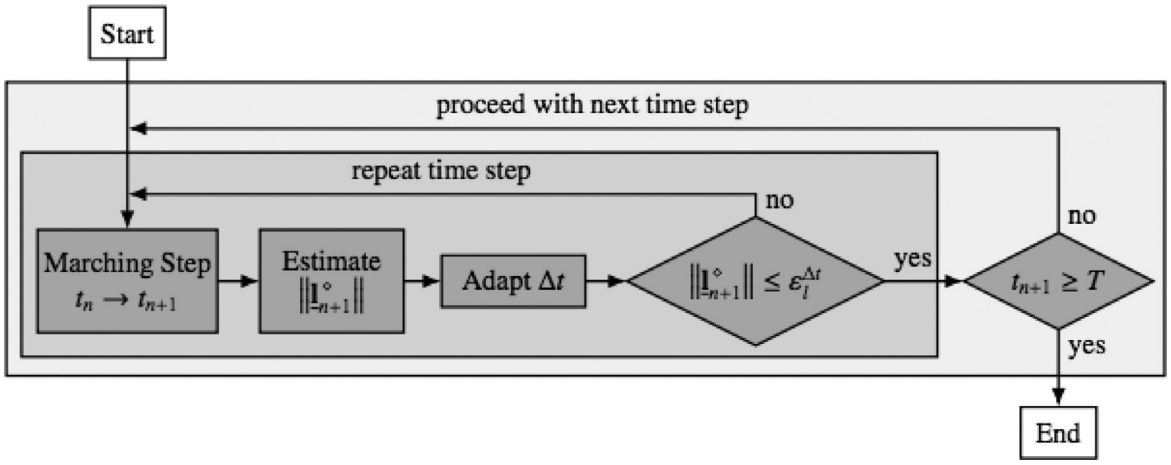


**Fig. 13.** Time Integration of FSI [108].

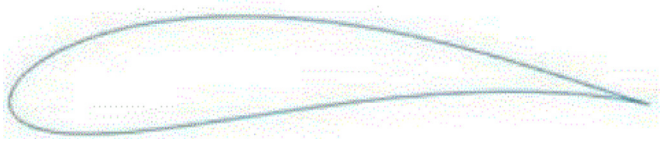

**Fig. 14.** Airfoil [114].

axial velocities induced by the rotor can be calculated. A FSI procedure combining BEMT theory and FE Analysis was presented by Suzuki and Mahfuz [119] by considering the interaction of hydrodynamic loads and structural responses within the inlet velocity, as well as lift and drag coefficients. Waqas and Ahmad [120] carried out a coupled modular FSI model for the evaluation of the tidal turbine performance and the stress loads under a uniform and unsteady flow (see Fig. 16), the FSI model resulted in 22.1% stress variation during a rotation cycle under steady flow conditions.

Bazilevs et al. [27] developed an FSI model to simulate both 2D and 3D vertical axis tidal turbine blades (VATT), to analyze the elastic response of the VATT in turbulent flow using anisotropic mesh adaptivity, and later compare the power co-efficient. A parametric analysis dealing with the effects of the inlet velocity and the mechanical behavior of the kinematic effect on a composite tidal current turbine was studied by Ye et al. [93] to investigate the effects of environmental conditions on the mechanical conditions of the composite under static and dynamic loading conditions. Suzuki and Mahfuz [121] compared the CFD & FSI Power Co-efficient values with the experimental values and concluded with the difference of less than 10% for the turbine performance, which was due to the difference in the pressure differences between each side of the blades.

## 7. Future development

Navier-Stokes equations are acknowledged as the mainstay for all fluid flow dynamics and their applications cover many areas such as FSI, aerodynamics, bio-inspired transportation, turbo machinery and nanofluids. Because of the omnipresent nature of the applications of the Navier-Stokes equations, researchers have increased interest in providing solutions to them (the equations). The mathematical complexity of the equations has made it necessary to solve them in three numerical ways: (i) fixed grid methods (ii) immersed boundary methods and (iii) mesh free methods. However, some researchers [11,12] have also noted that the Navier-Stokes equations do not take into account many other factors. For example, Goudarzi et al. [7] pointed out that the Navier-Stokes equations underestimate fluid forces as the rotations, changes in turbulence, and shear rate constitute additional forces. There is need for future studies to consider additional unsteady force, additional history force, additional rotational force and additional gradient force,

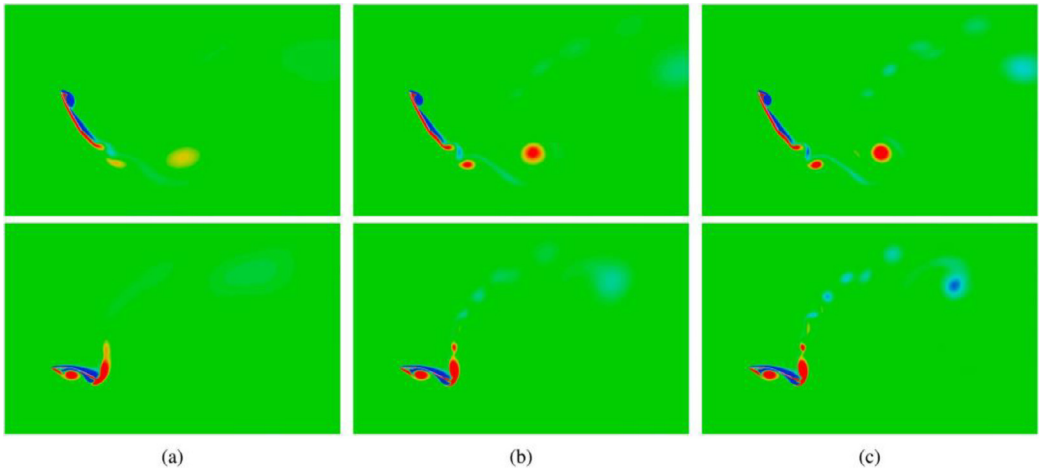


**Fig. 15.** Vorticity effects investigated for three different meshes (a) coarse mesh, (b) medium mesh, and (c) fine mesh [116].

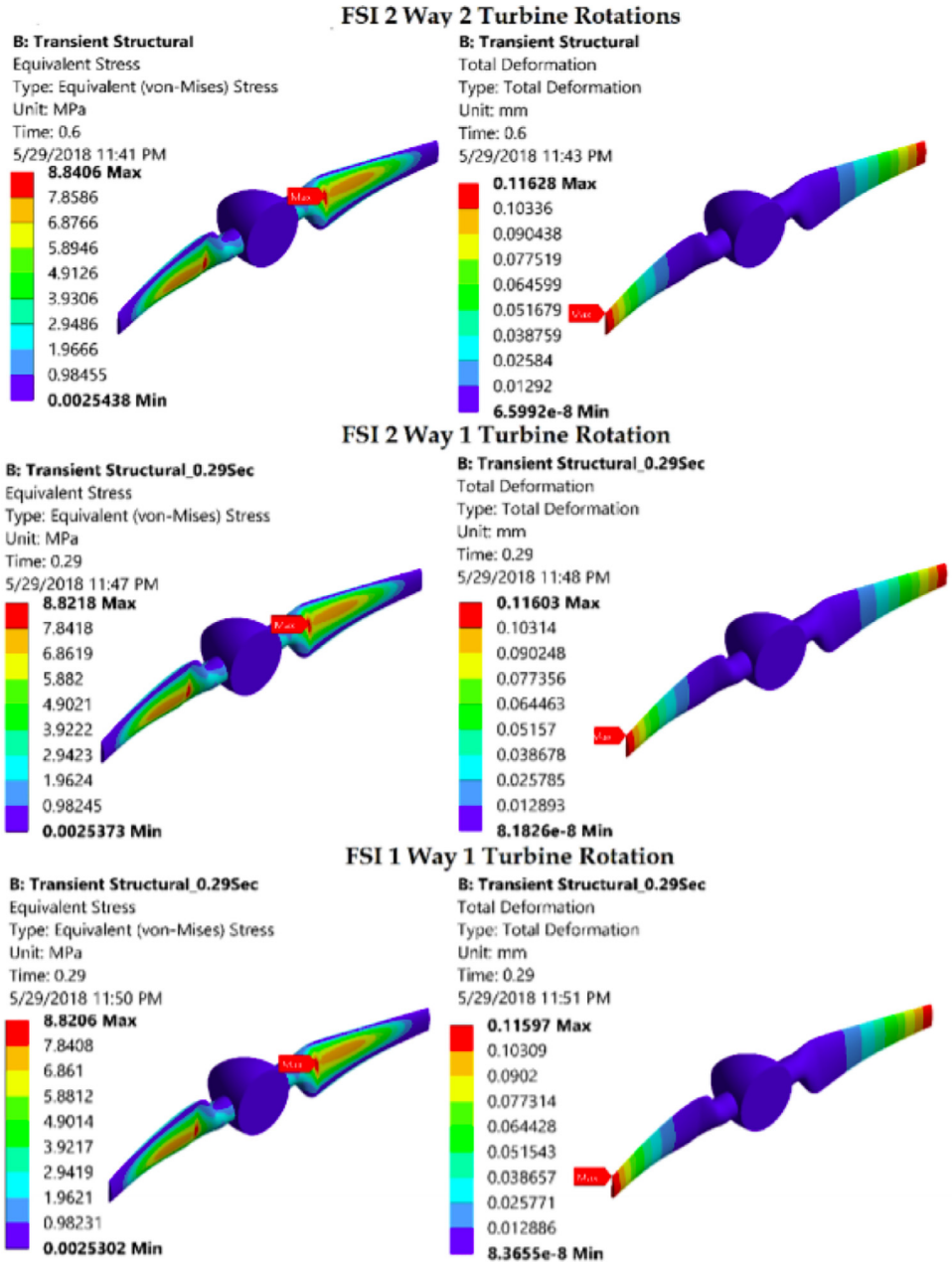


**Fig. 16.** Equivalent stress and total deformation on the tidal turbine rotor for three FSI simulations [122].

which is not the case with the Navier-Stokes's equations in their present forms.

Studies have also shown that even though the Navier-Stokes equations have been instrumental in the study of FSI, some critical aspects are overlooked. For example, Latifi et al. [40] assert that the flow is often also coupled with a source of vorticity such as pressure gradient because of non-slip boundary circumstances and Coriolis Effect and such flows are referred to as non-stationary. Latifi et al. [40] note that using the Riccati partial differential equation, the Navier-Stokes equations have been modified to include an approximate solution. When the flow gets turbulent, flow field fluctuation arises and gives rise to more unknowns. Another problem and consideration for future studies, therefore, is to close the existing equations; there is need to model more equations or modify the existing Navier-Stokes equations to introduce turbulence modeling.

Also, as there is an ardent need to use composite materials in the maritime industry to improve the structural and hydrodynamic performance of naval structures [123]. By using the FSI optimisation method this can be achieved. Along with the maritime industry, the Naval industry also has submerged structures which are subjected to the underwater shocks, and analysing the faults of such structures proves to be expensive [124]. Hence, by applying FSI based optimisation where a coupled FEA analysis with Cost Analysis can help reduce the costs by pre-estimating the faults.

Furthermore, the future work of this paper would include performing an innovative mathematical analysis to optimise the numerical performance of the tidal turbine blades base on the different time integration schemes where both the fluid and solid domains are present where the significant influence of stability would be place on the FSI coupling. Thus, by selecting the appropriate design parameters, and the objective functions the hydro-

dynamic efficiency of the tidal turbine blade could be improved. Finally, another area where the future development of this work could lead into the multi-objective hybrid model optimisation of the tidal turbine blade systems using a Genetic Algorithm coupled with FSI coupling based on the Finite Element Method parameters such as unsteady force and mass as the optimum objectives and constraints to develop a methodology for tidal energy to help improve the hydrodynamic efficiency and its ability in the future.

## 8. Conclusion

This perspective review has focused on low-order aerodynamic, Computational Fluid Dynamics (CFD) and structural modeling to explore Fluid Structure Interaction (FSI) based optimisation in tidal turbines. A comprehensive review on the FSI based optimisation in tidal turbines along with the detailed CFD & Structural modeling techniques and their applications in tidal turbines are presented. It has been acknowledged that, to aid humanity amidst the issue of using renewable or non-renewable sources of energy, practical solutions such as generating renewable energy from sustainable sources are effective. Tidal current energy is one such reliable solution but has also been found to be challenged by the concept of FSI. Hydrodynamic forces produce vibrations in the tidal current turbines which, in turn, cause resonance and dynamic loads on the turbines resulting in deformation and failure. The strains and stresses exerted on the structures are varied by the velocity and pressure of fluid flow and can cause either small or considerable deformations. A comprehensive insight is also provided into how the mathematical representations of models such as Actuator Disk Model, BEM and Vortex Model are derived. The fundamental governing equations of fluid dynamics have also been described as the cornerstone of CFD and these are the continuity, momentum, and energy equations. It is also found that currently there are only single parameter optimisation study presented on tidal turbines such as structural or hydrodynamic optimisation to improve either the airfoil or a 3D tidal turbine blade performance. More studies would be seen in the future to implement the FSI based optimisation by coupling with a Genetic Algorithm to demonstrate further applicability and help improve the hydrodynamic efficiency.

## Declaration of Competing Interest

The authors declare that they have no known competing financial interests or personal relationships that could have appeared to influence the work reported in this paper.

## References


[1] B. Kresning, M.R. Hashemi, S.P. Neill, J.A.M. Green, H. Xue, Energy 187 (2019) 115942, doi:10.1016/j.energy.2019.115942.
[2] Y. Liu, L. Tan, Renew. Energy 149 (2020) 42–54, doi:10.1016/j.renene.2019.12.017.
[3] H.B. Goh, S.H. Lai, M. Jameel, H.M. Teh, Energy 192 (2020) 116656, doi:10.1016/j.energy.2019.116656.
[4] M.K. Pine, P. Schmitt, R.M. Culloch, L. Lieber, L.T. Kregting, Renew. Sustain. Energy Rev. 103 (2019) 49–57, doi:10.1016/j.rser.2018.12.024.
[5] Y. Liu, L. Tan, Renew. Energy 148 (2020) 907–922, doi:10.1016/j.renene.2019.10.175.
[6] B. Mannion, S.B. Leen, S. Nash, Ocean Eng. 197 (2020) 106918, doi:10.1016/j.oceaneng.2020.106918.
[7] N. Goudarzi, M.H. Mohafez, W. Williams, in: Proceedings of the ASME Power Conference, 2019 V001T06A014.
[8] D. Cook, B. Davíðsdóttir, D.M. Kristófersson, Energy Sustain. Dev. 40 (2017) 126–138, doi:10.1016/j.esd.2017.07.007.
[9] C. Trivedi, M.J. Cervantes, Renew. Sustain. Energy Rev. 68 (2017) 87–101.
[10] L. Chen, F.L. Ponta, L.I. Lago, Energy Sustain. Dev. 15 (2011) 398–410, doi:10.1016/j.esd.2011.06.006.
[11] S. Nash, A. Phoenix, Renew. Sustain. Energy Rev. 80 (2017) 648–662.
[12] Y. Li, J. Yang, J. Song, Renew. Sustain. Energy Rev. 74 (2017) 19–25.
[13] P.M. Kumar, J. Seo, W. Seok, S.H. Rhee, A. Samad, Renew. Energy 135 (2019) 277–287, doi:10.1016/j.renene.2018.12.023.
[14] M. Fatehi, M. Nili-Ahmadabadi, O. Nematollahi, A. Minaiean, K.C. Kim, Renew. Energy 132 (2019) 773–785, doi:10.1016/j.renene.2018.08.047.
[15] H. Ullah, M. Hussain, N. Abbas, H. Ahmad, M. Amer, M. Noman, J. Ocean Eng. Sci. 4 (2019) 328–337, doi:10.1016/j.joes.2019.05.008.
[16] Z. Gao, T. Moan, L. Wan, C. Michailides, J. Ocean Eng. Sci. 1 (2016) 36–51, doi:10.1016/j.joes.2015.12.006.
[17] S. Narsipur, Low-Order Modeling of Dynamic Stall on Airfoils in Incompressible Flow, North Carolina State University, 2017.
[18] T.M. Sugathapala, S. Boteju, P.B. Withanage, S. Wijewardane, Energy Sustain. Dev. 59 (2020) 71–82, doi:10.1016/j.esd.2020.09.004.
[19] R.J.A.M. Stevens, L.A. Martinez-Tossas, C. Meneveau, Renew. Energy 116 (2018) 470–478.
[20] G.N. Barakos, T. Fitzgibbon, A.N. Kusyumov, S.A. KUSYUMOV, S.A. Mikhailov, Chin. J. Aeronaut. 33 (9) (2020) 2313–2328.
[21] A. Bottai, J.F. Horn, I. Oruc, J. Shipman, in: Proceedings of the AHS International Technical Meeting (Aeromechanics Design For Transformative Vertical Flight), 2018, p. 2018.
[22] M. Edmunds, A.J. Williams, I. Masters, A. Banerjee, J.H. VanZwieten, Energy 194 (2020) 116803, doi:10.1016/j.energy.2019.116803.
[23] C. Yan, Y. Gao, S. Zhao, S. Zhang, Y. Zhou, W. Deng, Z. Li, G. Jiang, L. Jin, G. Tian, T. Yang, X. Chu, D. Xiong, Z. Wang, Y. Li, W. Yang, J. Chen, Nano Energy 67 (2020) 104235, doi:10.1016/j.nanoen.2019.104235.
[24] K. Fan, M. Cai, F. Wang, L. Tang, J. Liang, Y. Wu, H. Qu, Q. Tan, Energy Convers. Manag. 198 (2019) 111820, doi:10.1016/j.enconman.2019.111820.
[25] G. Saini, R.P. Saini, Energy Sustain. Dev. 47 (2018) 94–106, doi:10.1016/j.esd.2018.09.005.
[26] H.A. Madsen, T.J. Larsen, G.R. Pirrung, L. Ang, F. Zahle, Wind Energy Sci. 5 (2020) 1–27.
[27] Y. Bazilevs, J. Yan, X. Deng, A. Korobenko, Arch. Comput. Methods Eng. 26 (2019) 1101–1115, doi:10.1007/s11831-018-9287-y.
[28] P. Yang, J. Xiang, F. Fang, C.C. Pain, Appl. Energy 236 (2019) 465–477.
[29] F. De Gregorio, A. Visingardi, Exp. Fluids 61 (2020) 179, doi:10.1007/s00348-020-03012-7.
[30] Y. Wang, Y. Gao, J. Liu, C. Liu, J. Hydrodyn. 31 (2019) 464–474, doi:10.1007/s42241-019-0032-2.
[31] P. Ouro, T. Stoesser, Comput. Fluids 152 (2017) 74–87.
[32] F. Yuan, G. Yan, R. Honerkamp, K.M. Isaac, M. Zhao, X. Mao, J. Wind Eng. Ind. Aerodyn. 190 (2019) 200–217, doi:10.1016/j.jweia.2019.05.001.
[33] A. Bulgac, Phys. Status Solidi 256 (2019) 1800592, doi:10.1002/pssb.201800592.
[34] S. Boroun, F. Larachi, Chem. Eng. J. 380 (2020) 122504, doi:10.1016/j.cej.2019.122504.
[35] A. Lindstrom, M. Amitay, AIAA J. 57 (2019) 2783–2794, doi:10.2514/1.J058135.
[36] M.A. Sayegh, J. Danielewicz, T. Nannou, M. Miniewicz, P. Jadwiszczak, K. Piekarska, H. Jouhara, Renew. Sustain. Energy Rev. 68 (2017) 1183–1192.
[37] P. Constantin, J. La, V. Vicol, Geom. Funct. Anal. 29 (2019) 1773–1793, doi:10.1007/s00039-019-00516-1.
[38] G. Katul, D. Li, C. Manes, WIREs Water 6 (2019) e1336, doi:10.1002/wat2.1336.
[39] A. Mollahosseini, S.A. Hosseini, M. Jabbari, A. Figoli, A. Rahimpour, Renew. Sustain. Energy Rev. 80 (2017) 774–788.
[40] M.S. Latifi, G. Colangelo, G. Starace, Exp. Comput. Multiph. Flow 2 (2020) 109–114, doi:10.1007/s42757-019-0045-7.
[41] A. Arabkoohsar, M. Khosravi, A.S. Alsagri, Int. J. Heat Mass Transf. 141 (2019) 432–443, doi:10.1016/j.ijheatmasstransfer.2019.06.101.
[42] F. Kuznik, K. Johannes, C. Obrecht, D. David, Renew. Sustain. Energy Rev. 94 (2018) 576–586.
[43] Q. Hou, E. D, S. Kuang, A. Yu, Fuel Process. Technol. 202 (2020) 106369, doi:10.1016/j.fuproc.2020.106369.
[44] M. Colombo, M. Fairweather, Chem. Eng. Sci. 195 (2019) 968–984, doi:10.1016/j.ces.2018.10.043.
[45] S. Song, Y.K. Demirel, M. Atlar, S. Dai, S. Day, O. Turan, Ocean Eng. 200 (2020) 107029, doi:10.1016/j.oceaneng.2020.107029.
[46] R. Kiran, R. Ahmed, S. Salehi, Chem. Eng. Res. Des. 153 (2020) 201–211, doi:10.1016/j.cherd.2019.10.012.
[47] J. Wu, H. Xiao, R. Sun, Q. Wang, J. Fluid Mech. 869 (2019) 553–586.
[48] S.K. Almeland, N.R.B. Olsen, K. Bråveit, P.R. Aryal, Eng. Appl. Comput. Fluid Mech. 13 (2019) 199–219, doi:10.1080/19942060.2019.1566094.
[49] Z. Yang, X. Cheng, X. Zheng, H. Chen, J. Therm. Sci. (2020), doi:10.1007/s11630-020-1339-6.
[50] J. Liu, W. Yang, M. Dong, A.L. Marsden, Comput. Methods Appl. Mech. Eng. 367 (2020) 113122, doi:10.1016/j.cma.2020.113122.
[51] H.M. Blackburn, D. Lee, T. Albrecht, J. Singh, Comput. Phys. Commun. 245 (2019) 106804, doi:10.1016/j.cpc.2019.05.015.
[52] A. Pakzad, Phys. D Nonlinear Phenom. 408 (2020) 132509, doi:10.1016/j.physd.2020.132509.
[53] S. Heinz, Phys. Fluids 31 (2019) 21702.
[54] S.T. Bose, G.I. Park, Annu. Rev. Fluid Mech. 50 (2018) 535–561.
[55] M. Shirzadi, P.A. Mirzaei, Y. Tominaga, Build. Simul. (2020), doi:10.1007/s12273-020-0657-7.
[56] A. Rezaeiha, H. Montazeri, B. Blocken, Energy Convers. Manag. 196 (2019) 1282–1298, doi:10.1016/j.enconman.2019.06.081.
[57] J. He, X. Jin, S. Xie, L. Cao, Y. Wang, Y. Lin, N. Wang, Renew. Energy 145 (2020) 2658–2670, doi:10.1016/j.renene.2019.07.132.
[58] Y. Du, B. Blocken, S. Pirker, Build. Environ. 170 (2020) 106604, doi:10.1016/j.buildenv.2019.106604.

[59] J.D. Smith, A. Suo-Antilla, V. Sreedharan, Fuel Process. Technol. 193 (2019) 187–196, doi:10.1016/j.fuproc.2019.05.010.
[60] R. Mereu, S. Passoni, F. Inzoli, Energy 187 (2019) 115969, doi:10.1016/j.energy.2019.115969.
[61] H. Lei, D. Zhou, Y. Bao, Y. Li, Z. Han, Energy Convers. Manag. 133 (2017) 235–248.
[62] B. Greschner, F. Thiele, M.C. Jacob, D. Casalino, Comput. Fluids 37 (2008) 402–413, doi:10.1016/j.compfluid.2007.02.013.
[63] M. Elkhoury, T. Kiwata, K. Nagao, T. Kono, F. ElHajj, Renew. Energy 129 (2018) 63–74, doi:10.1016/j.renene.2018.05.096.
[64] J. Su, H. Lei, D. Zhou, Z. Han, Y. Bao, H. Zhu, L. Zhou, Renew. Energy 141 (2019) 559–569, doi:10.1016/j.renene.2019.04.038.
[65] G. Bangga, P. Weihing, T. Lutz, E. Krämer, J. Mech. Sci. Technol. 31 (2017) 2359–2364, doi:10.1007/s12206-017-0432-6.
[66] X. Wang, H. Lei, Z. Han, D. Zhou, Z. Shen, H. Zhang, H. Zhu, Y. Bao, Atmos. Environ. 201 (2019) 173–189, doi:10.1016/j.atmosenv.2019.01.004.
[67] H. Li, Q. Huang, G. Pan, X. Dong, Ocean Eng. 203 (2020) 107224, doi:10.1016/j.oceaneng.2020.107224.
[68] S. Heinz, Prog. Aerosp. Sci. 114 (2020) 100597, doi:10.1016/j.paerosci.2019.100597.
[69] N. Renard, S. Deck, M.V. Salvetti, V. Armenio, J. Fröhlich, B.J. Geurts, H. Kuerten, in: Direct and Large-Eddy Simulation XI, Springer International Publishing, Cham, 2019, pp. 367–372.
[70] R. Angerbauer, T. Rung, Y. Hoarau, S.H. Peng, D. Schwamborn, A. Revell, C. Mockett, in: Progress in Hybrid RANS-LES Modeling, Springer International Publishing, Cham, 2020, pp. 367–377.
[71] O. Erkan, M. Özkan, T.H. Karakoç, S.J. Garrett, P.J. Thomas, Renew. Energy 161 (2020) 1359–1367, doi:10.1016/j.renene.2020.07.138.
[72] N. Weber, S. Landgraf, K. Mushtaq, M. Nimtz, P. Personnettaz, T. Weier, J. Zhao, D. Sadoway, Electrochim. Acta 318 (2019) 857–864, doi:10.1016/j.electacta.2019.06.085.
[73] M. Saleh Asheghabadi, M. Sahafnia, A. Bahadori, N. Bakhshayeshi, Int. J. Environ. Sci. Technol. 16 (2019) 2961–2972, doi:10.1007/s13762-018-2150-8.
[74] Z.J. Fu, Z.Y. Xie, S.Y. Ji, C.C. Tsai, A.L. Li, Ocean Eng. 195 (2020) 106736, doi:10.1016/j.oceaneng.2019.106736.
[75] C.T. Lee, J.B. Moody, R.E. Amaro, J.A. Mccammon, M.J. Holst, ACM Trans. Math. Softw. 45 (2019) 1–20.
[76] J. Sun, X. Sun, D. Huang, Energy 209 (2020) 118446, doi:10.1016/j.energy.2020.118446.
[77] Z. Ji, L. Fu, X. Hu, N. Adams, Comput. Methods Appl. Mech. Eng. 363 (2020) 112881, doi:10.1016/j.cma.2020.112881.
[78] A.B. Janjua, M.S. Khalil, M. Saeed, F.S. Butt, A.W. Badar, Energy Sustain. Dev. 58 (2020) 90–99, doi:10.1016/j.esd.2020.07.008.
[79] A. Muftah, SUSJ J. Sirte Univ. 9 (2019) 27–43.
[80] B. Yu, P. Hu, A.A. Saputra, Y. Gu, Appl. Math. Model. 89 (2021) 541–571, doi:10.1016/j.apm.2020.07.035.
[81] J. Li, C. Xu, J. Tichy, D.A. Borca-Tasciuc, J. Micromech. Microeng. 28 (2018) 85021.
[82] Y. Tang, G. Dong, Y.F. Zhao, Int. J. Adv. Manuf. Technol. 102 (2019) 4011–4030, doi:10.1007/s00170-019-03308-x.
[83] T.D. Economon, F. Palacios, J.J. Alonso, AIAA J. 53 (2015) 2437–2453.
[84] C. Kleinstreuer, Modern Fluid Dynamics, Springer, 2018.
[85] T.M. Berry, A. Ambaw, T. Defraeye, C. Coetzee, U.L. Opara, Food Bioprod. Process. 114 (2019) 43–59, doi:10.1016/j.fbp.2018.11.006.
[86] O. Zikanov, Essential Computational Fluid Dynamics, John Wiley & Sons, 2019.
[87] P.I. Muiruri, O.S. Motsamai, R. Ndeda, SN Appl. Sci. 1 (2019) 237, doi:10.1007/s42452-019-0254-5.
[88] J. Ožbolt, F. Oršanić, G. Balabanić, Struct. Infrastruct. Eng. 13 (2017) 135–146.
[89] V. Jaksic, C.R. Kennedy, D.M. Grogan, S.B. Leen, C.M.Ó. Brádaigh, P. Davies, Y.D.S. Rajapakse, in: Durability of Composites in a Marine Environment 2, Springer International Publishing, Cham, 2018, pp. 195–223, doi:10.1007/978-3-319-65145-3_11.
[90] F.L. Ponta, A.D. Otero, A. Rajan, L.I. Lago, Energy Sustain. Dev. 22 (2014) 3–12, doi:10.1016/j.esd.2014.04.004.
[91] G. Yu, Y. Ren, T. Zhang, W. Xiao, H. Jiang, China Ocean Eng. 32 (2018) 216–225, doi:10.1007/s13344-018-0023-z.
[92] E. Kementzetzidis, S. Corciulo, W.G. Versteijlen, F. Pisanò, Soil Dyn. Earthq. Eng. 120 (2019) 181–199, doi:10.1016/j.soildyn.2019.01.037.
[93] J. Ye, C. Chu, H. Cai, X. Hou, B. Shi, S. Tian, X. Chen, J. Ye, Compos. Struct. 212 (2019) 220–229, doi:10.1016/j.compstruct.2019.01.031.
[94] G.S. Payne, T. Stallard, R. Martinez, Renew. Energy. 107 (2017) 312–326, doi:10.1016/j.renene.2017.01.068.
[95] M. Nachtane, M. Tarfaoui, D. Saifaoui, A. El Moumen, O.H. Hassoon, H. Benyahia, Energy Rep. 4 (2018) 31–40, doi:10.1016/j.egyr.2018.01.002.
[96] B.W. Byrne, H.J. Burd, L. Zdravkovic, C.N. Abadie, G.T. Houlsby, R.J. Jardine, C.M. Martin, R.A. McAdam, M. Pacheco Andrade, A.M.G. Pedro, D.M. Potts, D.M.G. Taborda, Offshore Technol. Conf. 20 (2019), doi:10.4043/29373-MS.
[97] M. De Angelo, L. Placidi, N. Nejadsadeghi, A. Misra, Mech. Res. Commun. 103 (2020) 103462, doi:10.1016/j.mechrescom.2019.103462.
[98] M. Paradiso, F. Marmo, L. Rosati, Int. J. Solids Struct. 159 (2019) 90–110, doi:10.1016/j.ijsolstr.2018.09.021.
[99] H. Meng, F.S. Lien, G. Glinka, P. Geiger, Compos. Struct. 208 (2019) 678–701.
[100] A. Hashemian, E. Lakzian, A. Ebrahimi-Fizik, Comput. Math. Appl. 79 (2020) 1687–1705.
[101] Q.D. Nguyen, H.C. Park, T. Kang, J.H. Ko, Sci. Eng. Compos. Mater. 25 (n.d.) 1075–1083. 10.1515/secm-2017-0093.
[102] Y. Bazilevs, K. Takizawa, T.E. Tezduyar, M.C. Hsu, Y. Otoguro, H. Mochizuki, M.C.H. Wu, A. Grama, A.H. Sameh, in: Parallel Algorithms in Computational Science and Engineering, Springer International Publishing, Cham, 2020, pp. 195–233, doi:10.1007/978-3-030-43736-7_7.
[103] M. Ezkurra Mayor, J.A. Esnaola Ramos, M. Martinez Agirre, U. Lertxundi, U. Etxeberria, Analysis of One-Way and Two-Way FSI Approaches to Characterise the Flow Regime and the Mechanical Behaviour during Closing Manoeuvring Operation of a Butterfly Valve 12 (4) (2018) 409–415, doi:10.5281/zenodo.1316365.
[104] M. Sayed, T. Lutz, E. Krämer, S. Shayegan, R. Wüchner, J. Fluids Struct. 87 (2019) 354–377, doi:10.1016/j.jfluidstructs.2019.03.023.
[105] I. Marinić-Kragić, D. Vučina, Z. Milas, Energy 167 (2019) 841–852, doi:10.1016/j.energy.2018.11.026.
[106] E.L. Johnson, M.C. Hsu, Comput. Mech. 66 (2020) 311–322, doi:10.1007/s00466-020-01852-y.
[107] J.R. Wolmarans, K.J. Craig, AIP Conf. Proc. 2126 (1) (2019) 30064.
[108] J. Desrues, A. Argilaga, D. Caillerie, G. Combe, T.K. Nguyen, V. Richefeu, S. Dal Pont, Int. J. Numer. Anal. Methods Geomech. 43 (2019) 919–955.
[109] J. Jansson, N.C. Degirmenci, J. Hoffman, Int. J. Numer. Methods Biomed. Eng. 33 (2017) e2851, doi:10.1002/cnm.2851.
[110] S. Averweg, A. Schwarz, C. Nisters, J. Schröder, Comput. Methods Appl. Mech. Eng. 368 (2020) 113111, doi:10.1016/j.cma.2020.113111.
[111] T.A. Helgedagsrud, Y. Bazilevs, A. Korobenko, K.M. Mathisen, O.A. Øiseth, Comput. Fluids 179 (2019) 820–832, doi:10.1016/j.compfluid.2018.04.037.
[112] J. Yan, X. Deng, F. Xu, S. Xu, Q. Zhu, J. Appl. Mech. 87 (2020), doi:10.1115/1.4046317.
[113] B.J. Kim, H.G. Kim, Energies 13 (2020) 4876.
[114] M.A. Zullah, Y.H. Lee, Int. J. Fluid Mach. Syst. 11 (2018) 63–76, doi:10.5293/IJFMS.2018.11.1.063.
[115] S. Hoerner, S. Abbaszadeh, T. Maître, O. Cleynen, D. Thévenin, J. Fluids Struct. 88 (2019) 13–30, doi:10.1016/j.jfluidstructs.2019.04.011.
[116] G. Jeanmonod, M. Olivier, J. Fluids Struct. 70 (2017) 327–345, doi:10.1016/j.jfluidstructs.2017.01.009.
[117] T.D. Ivanov, A.M. Simonović, J.S. Svorcan, O.M. Peković, FME Trans. 45 (2017) 26–31, doi:10.5937/fmet1701026I.
[118] L. Daróczy, G. Janiga, D. Thévenin, Eng. Optim. 50 (2018) 1483–1499, doi:10.1080/0305215X.2017.1409350.
[119] T.J.R. Hughes, K. Takizawa, Y. Bazilevs, T.E. Tezduyar, M.C. Hsu, A. Grama, A.H. Sameh, in: Parallel Algorithms in Computational Science and Engineering, Springer International Publishing, Cham, 2020, pp. 151–193, doi:10.1007/978-3-030-43736-7_6.
[120] M. Waqas, N. Ahmad, J. Sci. Eng. (2020), doi:10.1007/s13369-020-04727-9.
[121] T. Suzuki, H. Mahfuz, Ships Offshore Struct. 13 (2018) 451–458, doi:10.1080/17445302.2017.1418621.
[122] M. Badshah, S. Badshah, K. Kadir, Energies 11 (2018) 1837.
[123] Y.L. Young, J. Fluids Struct. 24 (2008) 799–818, doi:10.1016/j.jfluidstructs.2007.12.010.
[124] S.J. Kim, M. Kõrgersaar, N. Ahmadi, G. Taimuri, P. Kujala, S. Hirdaris, Mar. Struct. 75 (2021) 102875, doi:10.1016/j.marstruc.2020.102875.